

RESEARCH ARTICLE **OPEN ACCESS**

# Aggregation of the Constitutively Active K296E Rhodopsin Mutant Contributes to Retinal Degeneration

Sreelakshmi Vasudevan  | Vivek Prakash  | Paul S.-H. Park 

Department of Ophthalmology and Visual Sciences, Case Western Reserve University, Cleveland, Ohio, USA

**Correspondence:** Paul S.-H. Park ([paul.park@case.edu](mailto:paul.park@case.edu))**Received:** 2 April 2025 | **Revised:** 18 June 2025 | **Accepted:** 7 July 2025**Funding:** This work was funded by grants from the National Institutes of Health (R01EY021731, P30EY011373, and UL1RR024989).**Keywords:** constitutive activity | G protein-coupled receptor | photoreceptor cell | phototransduction | protein aggregation | retinal degeneration**ABSTRACT**

A K296E mutation in rhodopsin causes autosomal dominant retinitis pigmentosa, a progressive retinal degenerative disease. Early characterizations of this mutation indicated that it causes the receptor to be constitutively active, which has been the primary focus when considering the pathogenic mechanism of the mutation thus far. Knockin mice expressing the K296E rhodopsin mutant were generated and characterized to better understand the pathogenic mechanism of the mutation. Knockin mice exhibited progressive retinal degeneration characteristic of retinitis pigmentosa. The K296E rhodopsin mutant mislocalized in photoreceptor cells and, surprisingly, appeared to aggregate, as indicated by the dye PROTEOSTAT, which binds protein aggregates. The propensity of the K296E rhodopsin mutant to aggregate was tested and confirmed *in vitro* but was dependent on the species background of rhodopsin. The K296E mutation on either murine or human rhodopsin backgrounds exhibited similar propensities to aggregate. The same mutation on a bovine rhodopsin background, however, exhibited a lower propensity to aggregate, indicating this species background does not adequately model the effects of the K296E mutation. In contrast to previous expectations, we demonstrate here that aggregation of the K296E rhodopsin mutant may contribute to photoreceptor cell loss in retinitis pigmentosa.

**1 | Introduction**

Rhodopsin is the light-activated G protein-coupled receptor expressed in rod photoreceptor cells of the retina. The rhodopsin gene is a hotspot for mutations, with over 100 mutations identified as a cause of retinitis pigmentosa (RP), a progressive retinal degenerative disease [1, 2]. Rhodopsin mutations have been classified clinically according to the severity of the retinal degeneration phenotype and molecularly based on the type of defect promoted in the receptor [3–5]. Mutations can cause a variety of molecular defects, with mutations causing receptor misfolding and aggregation forming the largest class of mutations [3]. The P23H mutation was the first identified mutation in patients with autosomal dominant RP (adRP) [6], and it is the most extensively characterized mutation both *in vitro* and *in vivo*. This point

mutation causes a moderate retinal degeneration phenotype and causes the receptor to misfold and aggregate [3, 4, 7].

Light activation of rhodopsin occurs via isomerization of 11-*cis* retinal, which is covalently linked to a lysine residue at position 296 of rhodopsin (Figure 1A). Activation of rhodopsin is terminated through regulatory mechanisms involving the phosphorylation of the receptor by rhodopsin kinase and the binding of arrestin [8]. A mutation of the lysine residue at position 296 to glutamic acid (K296E) is a cause of adRP with a more severe retinal degeneration phenotype with earlier onset compared to the phenotype promoted by the P23H mutation [9, 10]. Two types of molecular defects caused by the point mutation have been identified *in vitro*; however, only one has been demonstrated to occur *in vivo*. Initial *in vitro* characterization

This is an open access article under the terms of the [Creative Commons Attribution-NonCommercial-NoDerivs](https://creativecommons.org/licenses/by-nc-nd/4.0/) License, which permits use and distribution in any medium, provided the original work is properly cited, the use is non-commercial and no modifications or adaptations are made.

© 2025 The Author(s). *The FASEB Journal* published by Wiley Periodicals LLC on behalf of Federation of American Societies for Experimental Biology.

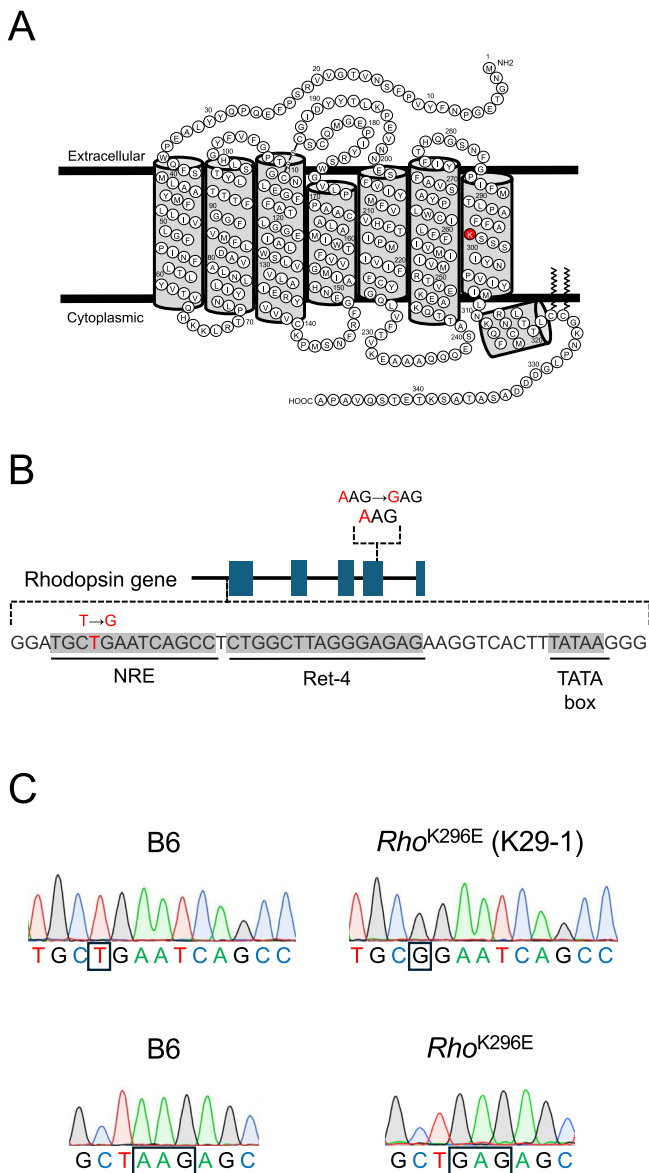


**FIGURE 1** | K296E mutation in rhodopsin. (A) Secondary structure of murine rhodopsin is shown with the lysine residue at position 296 highlighted in red. (B) The rhodopsin gene is illustrated highlighting the AAG (lysine) to GAG (glutamic acid) mutation in exon 4 present in K296E rhodopsin knockin mice and the promoter region shown highlighting a thymine (T) to guanine (G) base change within the NRE cis-regulatory element that is present in line K29-1. (C) Chromatograms obtained from sequencing genomic DNA of B6 and *Rho*<sup>K296E</sup> mice in the region of the NRE cis-regulatory element (top) or the region containing the codon at position 296 (bottom). The mutation positions are highlighted by the box.

of the K296E rhodopsin mutant demonstrated that the mutation causes the receptor to be constitutively active [11]. The constitutive activity of the K296E rhodopsin mutant was later demonstrated in vivo in a transgenic mouse model [12, 13]. The constitutive activity of the K296E mutant, however, did not result in persistent activation of the phototransduction cascade because of regulatory mechanisms involving arrestin, but rather resulted in stable interactions between the mutant and arrestin, which appeared to contribute to the retinal degeneration phenotype [12–14]. It has been unclear

why some mutations causing constitutive activity in rhodopsin lead to retinal degeneration and are classified as a cause of RP, whereas others lead to a more stationary form of night blindness and are classified as a cause of congenital stationary night blindness (CSNB) [8].

Other in vitro characterizations have suggested the possibility that the K296E rhodopsin mutant can also misfold and aggregate [15, 16]. This molecular defect, however, has not been demonstrated to occur in vivo. To determine whether the K296E rhodopsin mutation can promote misfolding and aggregation of the receptor and contribute to retinal degeneration, the mutant was characterized here both in vitro and in vivo. In vitro characterizations utilized a Förster resonance energy transfer (FRET)-based method in cells to detect aggregates of rhodopsin [17]. For in vivo characterizations, a knockin mouse expressing the K296E rhodopsin mutant was generated by CRISPR/Cas9 gene editing methods since previous in vivo studies utilized a transgenic mouse model [13]. In the current study, we demonstrate that the K296E rhodopsin mutant aggregates both in vitro and in vivo, and that the aggregation of the receptor can contribute to the retinal degeneration phenotype.

## 2 | Materials and Methods

### 2.1 | Mice

All animal studies reported here were conducted using protocols approved by the Institutional Animal Care and Use Committee at Case Western Reserve University School of Medicine. Mice were housed under cyclic 12h dark/12h light conditions. Both male and female mice were used for experiments. *Rho*<sup>K296E</sup> mice were generated using CRISPR/Cas9 gene targeting at the Case Transgenic and Targeting Facility of Case Western Reserve University School of Medicine (Cleveland, OH). Fertilized embryos from C57Bl/6J mice were injected with Cas9 nuclease (PNA Bio, Thousand Oaks, CA), sgRNA with the sequence 5'GAGCTCTTAGCAAAGAAAGC (PNA Bio, Thousand Oaks, CA) and ssDNA replacement oligonucleotide with the sequence 5'CACCCACCAGGGCT CCAACTTCGGCCCCATCTTCATGACTCTGCCAGCA TTCTTTGCTGAGAGCTCTTCCATCTATAACCCGGT CATCTACATCATGTTGAACAAGCAGGTGCCTGGGCT (Integrated DNA Technologies, Coralville, IA), which contained the lysine (AAG) to glutamic acid (GAG) mutation and introduced a conservative substitution for alanine (GCT to GCA). Deep sequencing was conducted on the MiSeq System (Illumina, San Diego, CA) by the Genomics Core at Case Western Reserve University School of Medicine (Cleveland, OH) on samples from mosaic founder mice to identify mice with the desired mutation. 3 founder mice harboring the mutation were identified, and each was backcrossed with C57Bl/6J mice for 10 generations to establish each line. A 10000 base pair region of the genome containing the rhodopsin gene and promoter region in these mice was sequenced by PCR-amplifying overlapping fragments to confirm that mice only exhibited changes introduced in the replacement oligonucleotide. C57Bl/6J (B6) mice were purchased from The Jackson Laboratory (Bar Harbor, ME). Transgenic mice that

were homozygous for the mutant G90D rhodopsin transgene on a null rhodopsin background ( $Rho^{TgG90D}$ ) were kindly provided by Dr. Paul Sieving (UC Davis, Sacramento, CA) [18].

## 2.2 | Quantifying Photoreceptor Cell Loss

Hematoxylin and eosin (H&E)-stained retinal sections were prepared by Excalibur Pathology (Norman, OK), imaged on an Axio Scan. Z1 Slide Scanner equipped with a Hitachi HV-F203 camera and a Plan Apo 20×/0.8-NA objective (Carl Zeiss Microscopy, White Plains, NY) or a Leica DME compound microscope equipped with an EC3 digital camera and 40×/0.65-NA objective (Leica Microsystems, Buffalo, NY), and the number of nuclei spanning the outer nuclear layer quantified and analyzed as described previously [7, 19]. Kinetics of photoreceptor cell loss were determined by fitting data by non-linear regression to a plateau followed by one phase decay equation in Prism 10 (GraphPad Software, San Diego, CA):  $y = \text{if}(x < x_0, y_0, \text{plateau} + (y_0 - \text{plateau}) \times e^{-k(-x_0+x)})$ . The variable  $y_0$  was fixed at 12 and *plateau* was set to be common among all data sets. Fitted values of the rate constant ( $k$ ) are reported with the standard error of the fit.

## 2.3 | Electroretinography (ERG)

Mice were dark-adapted overnight and ERG conducted under scotopic and photopic conditions on a Celeris rodent ERG system (Diagnosys, Lowell, MA), as described previously [7]. The a-wave and b-wave amplitudes from ERG traces obtained at different intensities of white light were plotted and fit by non-linear regression in Prism 10 (GraphPad Software, San Diego, CA) to a standard dose-response model (scotopic a-wave and photopic b-wave),  $R = \frac{R_{\max}}{1 + 10^{\log K_A - \log I}}$ , or biphasic dose-response model (scotopic b-wave),  $R = \frac{R_{\max} \times f}{1 + 10^{\log K_A - \log I}} + \frac{R_{\max} \times (1-f)}{1 + 10^{\log K_B - \log I}}$ .  $R$  is the amplitude of the a-wave or b-wave at a given flash intensity ( $I$ ),  $R_{\max}$  is the maximal amplitude at a saturating flash intensity,  $K_A$  and  $K_B$  represents the flash intensity that generates a half-maximal amplitude,  $f$  is the fraction of the curve that has  $K_A$ .

## 2.4 | Rhodopsin Expression

RT-qPCR was conducted on the LightCycler 96 Real-Time PCR System (Roche Diagnostics, Indianapolis, IN) to quantify rhodopsin transcripts in retinal extracts. Sample preparation, primers for rhodopsin, *Gnat1*, and 18s rRNA transcripts, and qPCR procedures and analyses are the same as those described previously [7, 20]. Rhodopsin protein levels in retinal extracts from mice were quantified by western blot analysis. Preparation of retina samples, SDS-PAGE using Novex 4%–12% Tris-glycine gels (Invitrogen, Camarillo, CA), western blotting procedures, and quantification of bands on western blots by the Odyssey Fc Imaging System (LI-COR Biosciences, Lincoln, NE) were performed, as described previously [7]. Primary antibodies against rhodopsin (anti-1D4) [21], GAPDH (Cat. No. 10494-1-AP; Proteintech, Rosemont, IL), and GNAT1 (Cat. No. GTX105960, Gene Tex Inc., Irvine, CA) and IRDye 800CW donkey anti-mouse (Cat. No. 926-32212) or IRDye 680LT donkey anti-rabbit

(Cat. No. 925-68023) secondary antibodies (LI-COR Biosciences, Lincoln, NE) were used.

## 2.5 | Labeling of Retinal Cryosections and Confocal Microscopy

Retinal cryosection preparation, immunohistochemistry, TUNEL assay, PROTEOSTAT labeling, confocal microscopy, and analysis and processing of images were conducted essentially as described previously [7, 22, 23]. Rhodopsin was labeled with an anti-4D2 (Cat. No. MABN15, MilliporeSigma, Burlington, MA) primary antibody and Alexa Fluor 647 goat anti-mouse secondary antibody (Cat. No. A21237, Thermo Fisher Scientific, Waltham, MA). Peripherin was labeled with anti-PRPH2 primary antibody (Cat. No. 18109-1-AP, Proteintech, Rosemont, IL) and sodium/potassium-ATPase  $\alpha 3$  was labeled with anti-ATP1A3 primary antibody (Cat. No. 10868-1-AP, Proteintech, Rosemont, IL). These antibodies were detected with the Alexa Fluor 568 goat anti-rabbit secondary antibody (Cat. No. A-11011, Thermo Fisher Scientific, Waltham, MA). An antigen retrieval step was included prior to labeling with anti-PRPH2 and anti-ATP1A4 antibodies, which included incubation of cryosections in 10mM Tris-HCl (pH9) at 60°C for 10 min and then at room temperature for 30 min [7]. TUNEL assay was conducted using the One-step TUNEL In Situ Apoptosis Kit (Cat. No. E-CK-A324, Elabscience, Houston, Tx). PROTEOSTAT labeling was conducted using the PROTEOSTAT Aggresome Detection Kit (Enzo Life Sciences, Farmingdale, NY).

Confocal microscopy was performed on an Olympus FV1200 IX83 laser scanning confocal microscope (Evident Scientific, Waltham, MA) using either a UPlanXApo 40×/1.40 NA oil objective or UPLXAPO 100×/1.45 NA objective. Labeled cryosections were cover-slipped with DAPI Fluoromount-G mounting media (Southern Biotech, Birmingham, AL) for 40× imaging or with ProLong Glass Antifade Mountant with NucBlue stain (Invitrogen, Carlsbad, CA) for 100× imaging. DAPI and NucBlue were detected with 405 nm diode laser excitation and 425–460 nm emission; Alexa Fluor 647 and TUNEL positive cells were detected with 635 nm diode laser excitation and 655–755 nm emission; and Alexa Fluor 568 and PROTEOSTAT dye were detected by 559 nm diode laser excitation and 575–620 nm emission. Deconvolution, maximum projection image generation, and surface rendering were performed in Huygens Essential 23.10 software (Scientific Volume Imaging, Hilversum, Netherlands), as described previously [23]. TUNEL, PROTEOSTAT, and DAPI positive cells were quantified from 40× confocal microscopy images (317×317  $\mu\text{m}$ ) using ImageJ (version 1.53n) [24], as described previously [7]. Co-labeling of nuclei by TUNEL and PROTEOSTAT was quantified from 100× confocal microscopy images (2 regions of 127×127  $\mu\text{m}$ ) using the Coloc 2 plugin in Fiji (version 2.1.0/1.53c) [25], as described previously [23].

## 2.6 | Characterization of Aggregation In Vitro in HEK293 Cells

DNA constructs coding for murine, human, and bovine rhodopsin with a yellow fluorescent protein (YFP) variant or

mTurquoise2 (mTq2), both tagged with a 1D4 epitope, were described previously [7, 26–28]. The K296E mutation was introduced into each of these constructs adapting procedures in the QuickChange II Site-Directed Mutagenesis Kit (Agilent Technologies, Santa Clara, CA) using the following forward and reverse primers: murine rhodopsin, 5'-ACTCTGCCAGC TTTCTTTGCTGAGAGCTCTTCCA and 5'-TGGAAGAGCT CTCAGCAAAGAAAGCTGGCAGAGT; human rhodopsin, 5'-CAGCGTCTTTGCCGAGAGCGCCGATC and 5'-G ATGGCGGCGCTCTCGCAAAGAAGCTG; bovine rhodopsin 5'-CCGGCTTTCTTTGCCGAGACTTCTGCCGTCT and 5'-AGACGGCAGAAGTCTCGCAAAGAAAGCCGG. The K296M mutation was introduced into the human rhodopsin constructs using the following forward and reverse primers: 5'-GCGTCTTTGCCATGAGCGCCGATC and 5'-GATGGCGGCGCTCATGGCAAAGAAGCG. HEK293T/17 cells (Cat. No. CRL-11268, American Type Culture Collection, Manassas, VA) were cotransfected with constructs coding for YFP- and mTq2-tagged rhodopsins, and a FRET assay was conducted on a FluoroMax-4 or FluoroMax Plus spectrofluorometer (Horiba Jobin Yvon, Edison, NJ), as described previously [17]. Total, *n*-dodecyl- $\beta$ -D-maltoside (DM)-sensitive, and DM-insensitive FRET signals were computed and FRET curves generated by plotting the FRET efficiency versus the acceptor: donor (A:D) ratio and fitting the data by non-linear regression to a rectangular hyperbolic function using Prism 10 (GraphPad Software, San Diego, CA):  $E = (E_{\max} \times A:D) / (EC_{50} + A:D)$  [17]. The non-specific FRET  $E_{\max}$  was defined previously [27].

## 2.7 | Statistics

All statistical analyses were conducted using Prism 10 (GraphPad Software, San Diego, CA), including ANOVA and post hoc analysis and extra sum of squares *F* tests.

## 3 | Results

### 3.1 | Generation and Initial Characterization of K296E Rhodopsin Knockin Mice

A knockin mouse that expresses the K296E rhodopsin mutant was generated by CRISPR/Cas9 gene editing methods to study the mutant in vivo. Knockin mice have proven to be a more accurate model of adRP compared to transgenic mice, where the expression of mutants can be variable [29]. A guide RNA was selected so that Cas9 endonuclease would cut the rhodopsin gene in exon 4 in the vicinity of the sequence corresponding to codon 296. Homology directed repair in the presence of a replacement oligonucleotide introduced the lysine (AAG) to glutamic acid (GAG) mutation at codon position 296 (Figure 1B,C). Three founder mice (K29-1, K29-4, and K29-21) were identified that contained the AAG to GAG mutation, and lines were established for each. The rhodopsin gene, including the promoter region, was sequenced for each of the three lines. No sequence changes were identified in the K29-4 and K29-21 lines except for those introduced by the replacement oligonucleotide. Samples from the K29-1 line, however, exhibited a thymine (T) to guanine (G) base change within the NRE cis-regulatory element in the rhodopsin promoter region (Figure 1B,C).

The retinal phenotype was characterized in each of these lines in both heterozygous (*Rho*<sup>K296E/+</sup>) and homozygous (*Rho*<sup>K296E</sup>) backgrounds. The loss of photoreceptor cells was quantified by counting the number of nuclei spanning the outer nuclear layer. All three lines exhibited the loss of photoreceptor cells, with the loss in *Rho*<sup>K296E</sup> mice more severe than that in *Rho*<sup>K296E/+</sup> mice (Figure 2). The level of photoreceptor cell loss was less severe in the K29-1 line compared to the other two lines in both heterozygous and homozygous backgrounds. The K29-4 and K29-21 lines exhibited similar levels of photoreceptor cell loss. Thus, the mutation in the promoter region present in the K29-1 line appears to diminish the effect of the mutation.

### 3.2 | Expression of Rhodopsin in K296E Rhodopsin Knockin Mice

To determine if the mutation in the promoter region present in the K29-1 line impacts the expression of rhodopsin, RT-qPCR and western blot analysis were conducted on retinal samples from 2-week-old heterozygous and homozygous mice to quantify the levels of rhodopsin transcript and protein. Rhodopsin was normalized to *18s rRNA* or GAPDH, which does not consider any photoreceptor cell loss, and transducin transcripts (*Gnat1*) or protein (GNAT1), which would take into account photoreceptor cell loss. In heterozygous mice, the level of rhodopsin transcripts was similar to wild-type (WT) C57Bl/6J (B6) mice regardless of normalization to *18s rRNA* or *Gnat1* for all three mouse lines (Figure 3A), which indicates that loss of photoreceptor cells is likely minimal at this age. The level of rhodopsin protein, as assessed by western blot (e.g., Figure 3B,E), was a little less than half of that in B6 mice when normalized to GAPDH and higher when normalized to GNAT1 (Figure 3C), which indicates that photoreceptor cells are affected even if photoreceptor cell loss is minimal at this early age. Significant differences were not observed in the level of rhodopsin protein among the three lines.

In homozygous mice, rhodopsin transcript levels were lower compared to that in B6 mice for all three lines (Figure 3D). Homozygous mice exhibited differences in rhodopsin transcript levels when normalized to *18s rRNA* or *Gnat1*, which suggests there is a loss of photoreceptor cells at this early age. Rhodopsin transcript levels in Line K29-1 were a little higher than that in the other two lines when normalized to *18s rRNA*, but all three lines exhibited similar levels of rhodopsin transcripts when normalized to *Gnat1*. Even when photoreceptor loss was taken into account by normalization to *Gnat1*, rhodopsin transcript levels were only about half of that for B6 mice, indicating that transcription is affected in these mutant mice. While 2-week-old homozygous mice from line K29-4 exhibit significant photoreceptor cell loss, appreciable photoreceptor cell loss is not apparent in homozygous mice from line K29-1 (Figure S1). Thus, retinal degeneration may affect transcription of rhodopsin in line K29-4, as was the case in homozygous mice expressing the P23H or G188R rhodopsin mutants [7]. The lower level of rhodopsin transcripts in line K29-1 cannot be explained by photoreceptor cell loss but may be a result of the mutation in the rhodopsin promoter region.

The level of the K296E rhodopsin mutant protein expressed in homozygous mice was lower than that of rhodopsin in B6

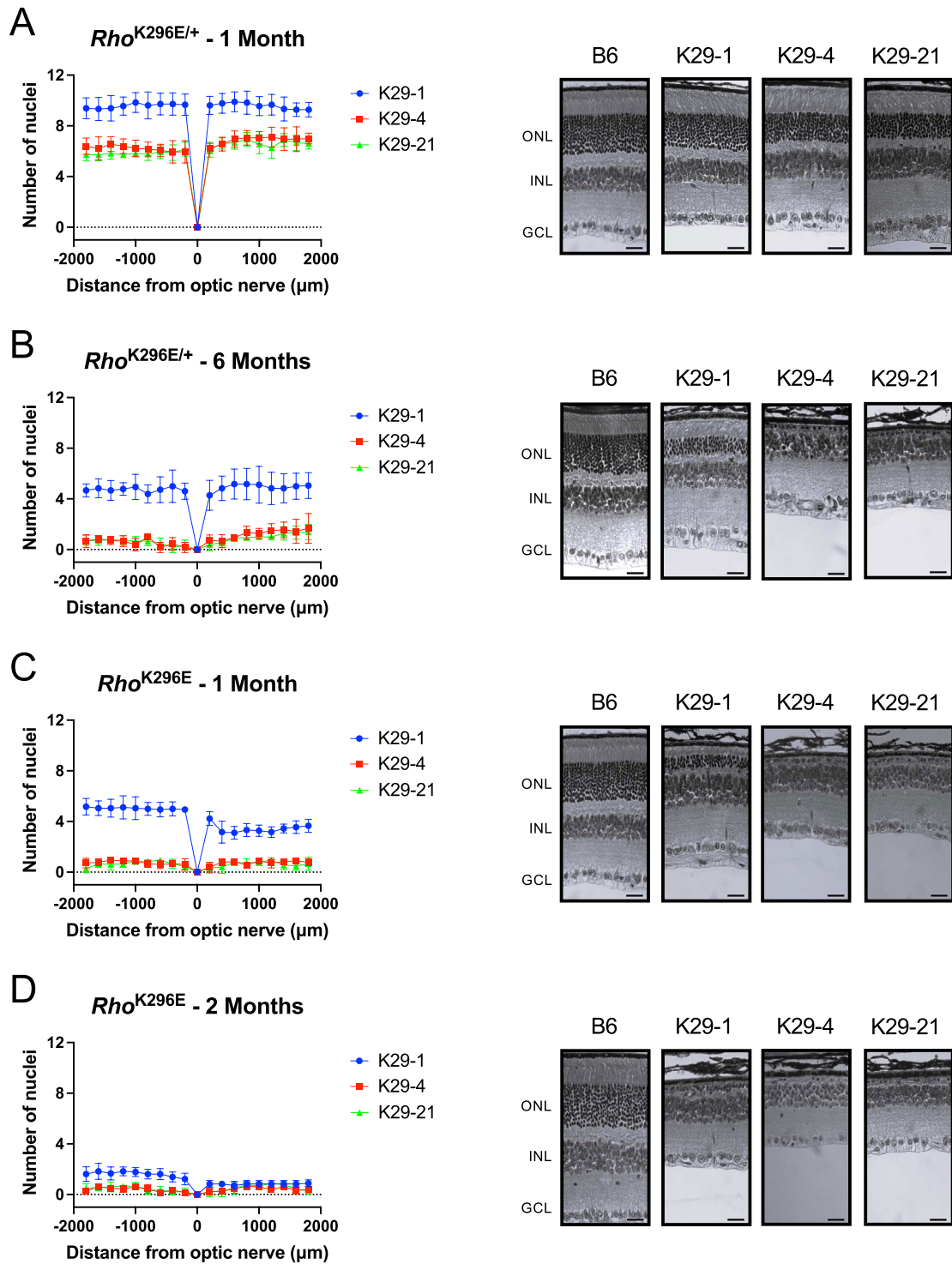


**FIGURE 2** | Photoreceptor cell loss in K296E rhodopsin knockin mice. Spider plots quantifying the number of photoreceptor cell nuclei in the inferior (negative) and superior (positive) regions of the retina of 1-month (A) and 6-month-old (B) *Rho*<sup>K296E/+</sup> mice or 1-month (C) and 2-month-old (D) *Rho*<sup>K296E</sup> mice are shown on the left-hand side. Data are shown for K29-1, K29-4, and K29-21 lines and age of mice are indicated. The mean and standard deviation are shown at different distances from the optic nerve ( $n=6$ ). Corresponding images of retinal sections are shown on the right-hand side for B6 mice and the K29-1, K29-4, and K29-21 lines. The outer nuclear layer (ONL), inner nuclear layer (INL), and ganglion cell layer (GCL) are labeled. Scale bar, 25  $\mu\text{m}$ .

mice (Figure 3F). Like in heterozygous mice, rhodopsin levels normalized to GNAT1 were higher than rhodopsin levels normalized to GAPDH, which is consistent with the loss of photoreceptor cells occurring in homozygous mice, at least in lines K29-4 and K29-21. In contrast to heterozygous mice, the level of

the K296E rhodopsin mutant in homozygous mice in line K29-1 was lower than that in lines K29-4 and K29-21. The level of the mutant was about 2-fold lower when normalized to GAPDH and 4-fold lower when normalized to GNAT1. In lines K29-4 and K29-21, the level of rhodopsin was only about 20% of that in B6

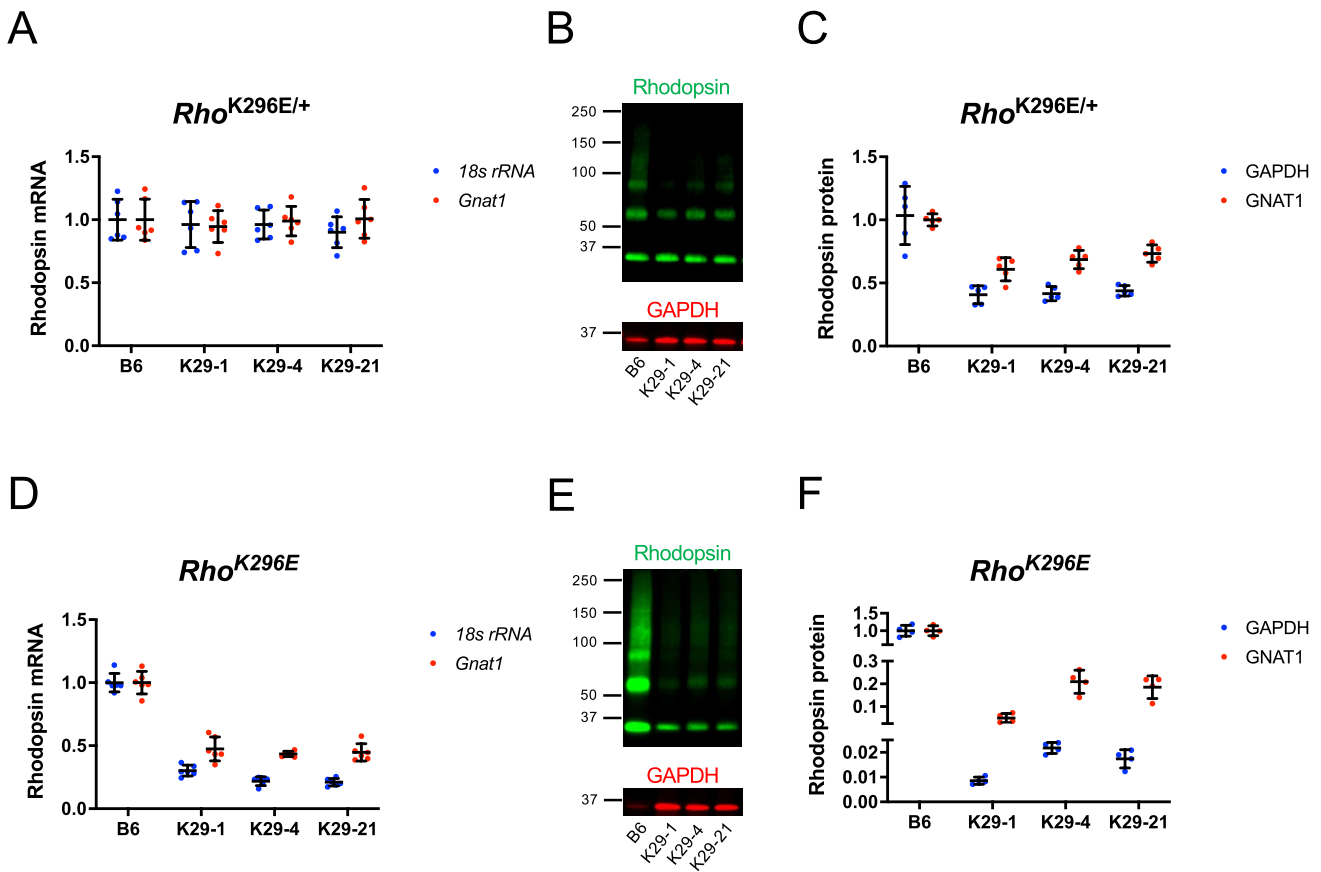


**FIGURE 3** | Rhodopsin expression in K296E rhodopsin knockin mice. Rhodopsin transcripts and protein were quantified from the retina of 2-week-old *Rho*<sup>K296E/+</sup> (A–C) and *Rho*<sup>K296E</sup> mice (D–F) from lines K29-1, K29-4, and K29-21. (A, D) Rhodopsin transcripts in *Rho*<sup>K296E/+</sup> (A) and *Rho*<sup>K296E</sup> (D) mice were quantified by RT-qPCR and expressed relative to the mean value for B6 mice and normalized to *18s rRNA* (blue) or *Gnat1* (red). Individual data points are shown and are plotted along with the mean and standard deviation ( $n=6$ ). Statistical analyses are reported in Table S1. (B, E) Western blots of retinal extracts from *Rho*<sup>K296E/+</sup> (B) and *Rho*<sup>K296E</sup> (E) mice labeled with anti-1D4 (green) and anti-GAPDH (red) antibodies. Molecular weight markers are indicated in kDa. (C, F) Rhodopsin protein was quantified from western blots (e.g., Figure 3B,E, Figure S2). The intensity of bands in western blots corresponding to rhodopsin were normalized to the intensity of the band corresponding to GAPDH (blue) or GNAT1 (red) and expressed relative to the mean value for B6 mice. Individual data points are shown along with the mean and standard deviation (*Rho*<sup>K296E/+</sup>,  $n=5$ ; *Rho*<sup>K296E</sup>,  $n=4$ ). Statistical analyses are reported in Table S2.

mice when normalized to GNAT1. Taken together, most of the K296E rhodopsin mutant appears to be degraded, and the mutation in the promoter region of line K29-1 appears to reduce the expression of the K296E rhodopsin mutant relative to that in lines K29-4 and K29-21.

### 3.3 | Characterization of Photoreceptor Cell Loss Promoted by K296E Mutant Rhodopsin

The K29-4 line was investigated from this point on to better understand the effect of the K296E rhodopsin mutation in photoreceptor cell loss, and is the line referred to as *Rho*<sup>K296E/+</sup> and *Rho*<sup>K296E</sup> mice from this point onwards. Spider plots of the number of nuclei spanning the outer nuclear layer were generated for 2 week to 6-month-old *Rho*<sup>K296E/+</sup> mice (Figure 4A) and 2 week to 2-month-old *Rho*<sup>K296E</sup> mice (Figure 4B). The degeneration was more severe in the inferior retina in *Rho*<sup>K296E/+</sup> mice compared to that in the superior retina. The kinetics of the photoreceptor cell loss was determined for the central region of the superior and

inferior retina (Figure 4C). The rate of photoreceptor cell loss was about 2-fold faster in the inferior retina of *Rho*<sup>K296E/+</sup> mice compared to that in the superior retina. In contrast, the rate of photoreceptor cell loss was similar in the superior and inferior retina of *Rho*<sup>K296E</sup> mice. The rate of photoreceptor cell loss in *Rho*<sup>K296E</sup> mice was 6-fold faster or more compared to that in *Rho*<sup>K296E/+</sup> mice.

The functional changes accompanying the loss of photoreceptor cells in *Rho*<sup>K296E/+</sup> and *Rho*<sup>K296E</sup> mice were characterized by electroretinography (ERG) in 1-month-old mice (Figure 4D–F). In *Rho*<sup>K296E/+</sup> mice, the maximal amplitude ( $R_{max}$ ) in both the scotopic a-wave and photopic b-wave response (Figure 4D,F), which reflect rod and cone photoreceptor cell function [30–32], respectively, was lower without a significant change in the  $K_A$  (intensity generating half-maximal amplitude). The scotopic b-wave response in *Rho*<sup>K296E/+</sup> mice reflected these changes in rod and cone photoreceptor cell function (Figure 4E). Thus, both rod and cone photoreceptor cell function were affected in 1-month-old *Rho*<sup>K296E/+</sup> mice. The scotopic and photopic ERG response was essentially eliminated in *Rho*<sup>K296E</sup> mice, indicative

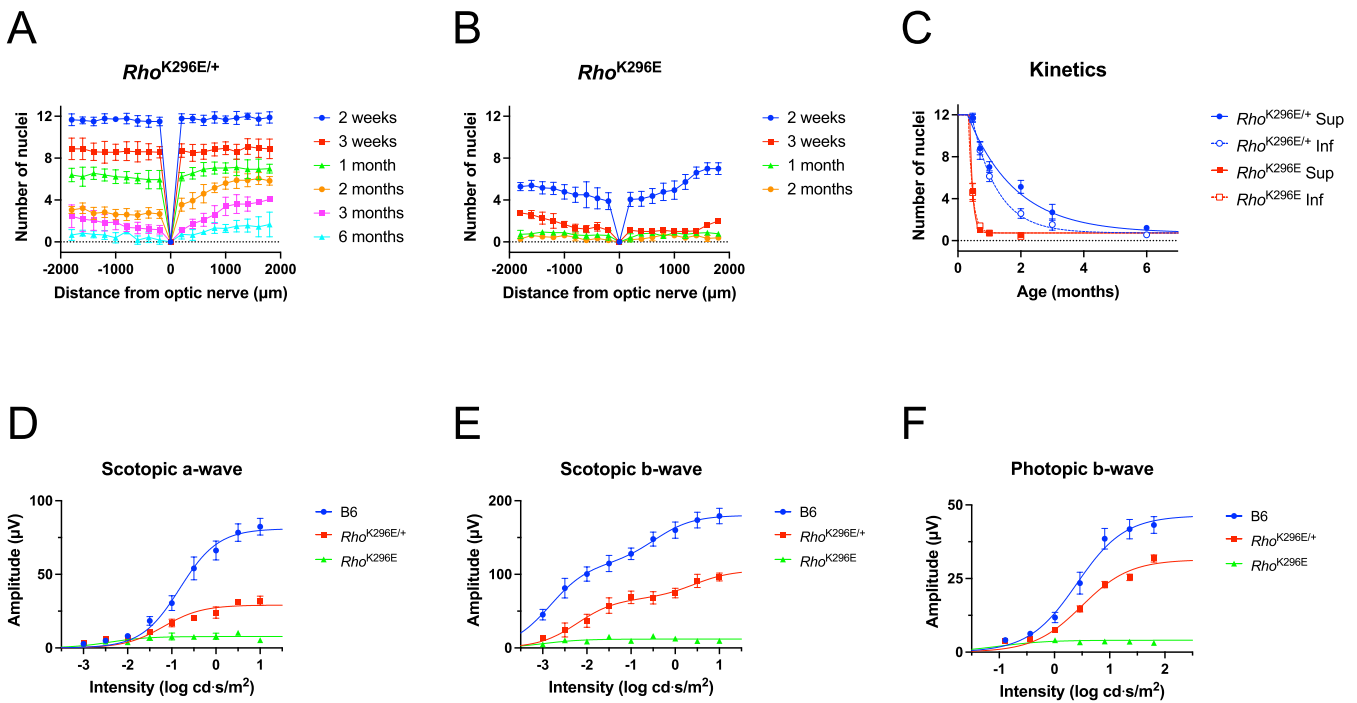


**FIGURE 4** | Progressive photoreceptor cell loss in  $Rho^{K296E/+}$  and  $Rho^{K296E}$  mice. (A, B) Spider plots. The number of photoreceptor cell nuclei in the inferior (negative) and superior (positive) regions of the retina were quantified in retinal section images (e.g., Figure 2) from  $Rho^{K296E/+}$  (A) and  $Rho^{K296E}$  (B) mice at the indicated ages. The mean and standard deviation are shown at different distances from the optic nerve ( $n=6$ ). (C) Kinetics of photoreceptor cell loss. Mean values of the number of photoreceptor cell nuclei, and their associated standard deviation, are plotted as a function of age in the superior (solid symbol) or inferior (open symbol) region of the retina in  $Rho^{K296E/+}$  (blue) and  $Rho^{K296E}$  (red) mice ( $n=6$ ). Data were fit by non-linear regression to determine the rate constants, which are reported in Table S3. (D–F) ERG response from 1-month-old B6,  $Rho^{K296E/+}$  and  $Rho^{K296E}$  mice. The amplitude of the scotopic a- (D) and b-wave (E) and photopic b-wave (F) are plotted as a function of the intensity of light stimulus. Mean values are plotted with the standard error (B6,  $n=10$ ;  $Rho^{K296E/+}$ ,  $n=8$ ;  $Rho^{K296E}$ ,  $n=8$ ). Data were fit by non-linear regression and fitted values are reported in Table S4 and statistical analyses reported in Table S5.

of the more severe loss of photoreceptor cells exhibited in these mice (Figures 2C and 4B).

### 3.4 | Mislocalization and Aggregation of K296E Mutant Rhodopsin in Photoreceptor Cells

The localization of rhodopsin within photoreceptor cells was characterized by immunohistochemistry in 2-week-old mice using the anti-4D2 antibody (Figure 5A), which detects the amino terminal region of rhodopsin [33]. B6 mice exhibited staining by the anti-4D2 antibody only in the rod outer segment, demonstrating that WT rhodopsin is properly targeted without mislocalization. In contrast, the anti-4D2 antibody detected mislocalized rhodopsin in the outer nuclear layer in both  $Rho^{K296E/+}$  and  $Rho^{K296E}$  mice. To examine more precisely the localization of rhodopsin within the outer and inner segments of rod photoreceptor cells, retinal cryosections were co-labeled with the anti-4D2 antibody and either anti-peripherin (PRPH2) or anti-sodium/potassium-ATPase  $\alpha 3$  (ATP1A3) antibodies, which detect markers for the outer segment and inner segment of rod photoreceptor cells, respectively [34]. In B6 mice, colocalization was detected between rhodopsin and PRPH2 in the outer segment but was absent between rhodopsin and ATP1A3 in the inner segment of photoreceptor cells (Figure 6). In  $Rho^{K296E/+}$  mice, colocalization was detected between rhodopsin and PRPH2 in shortened outer segments, and sporadic

colocalization was detected between rhodopsin and ATP1A3 in the inner segments. In  $Rho^{K296E}$  mice, there was little colocalization between rhodopsin and PRPH2, and labeling of PRPH2 in the photoreceptor cells was limited (Figure 6A), indicating that the outer segments are largely disrupted. Rhodopsin did colocalize with ATP1A3 (Figure 6B), indicating that the K296E rhodopsin mutant is present in the inner segment of rod photoreceptor cells in addition to the outer nuclear layer.

Mislocalization of misfolding mutants of rhodopsin in the outer nuclear layer is accompanied by aggregation of the mutants, which can be detected in retinal cryosections by the dye PROTEOSTAT [7, 23], a molecular rotor dye that detects aggregated proteins [35]. To determine if the mislocalization of the K296E rhodopsin mutant is accompanied by aggregation of the mutant, retinal cryosections from  $Rho^{K296E/+}$  mice were labeled with PROTEOSTAT. PROTEOSTAT labeling was observed in the outer nuclear layer (Figure 5B), indicating that the mutant aggregates. To determine if aggregation, detected by PROTEOSTAT, occurs with other constitutively active rhodopsin mutants, a transgenic mouse expressing the G90D rhodopsin mutant on a null rhodopsin background ( $Rho^{TgG90D}$ ) was examined [18]. The G90D rhodopsin mutant is constitutively active and is classified as a cause of CSNB but can also cause mild retinal degeneration [20, 36–38]. Labeling retinal cryosections with the anti-4D2 antibody or PROTEOSTAT did not detect any mislocalization of rhodopsin or PROTEOSTAT-positive photoreceptor cell nuclei (Figure 5B). Thus, not all

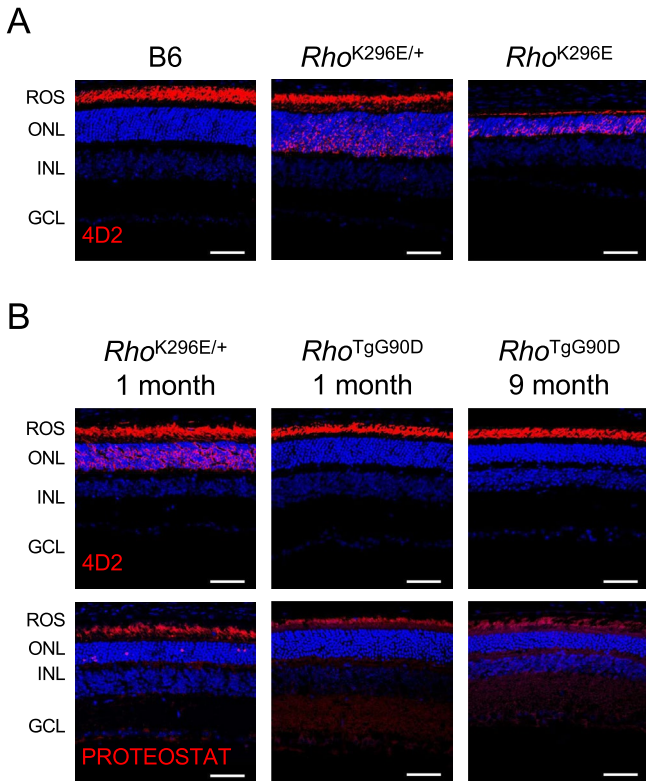


**FIGURE 5** | Mislocalization and aggregation of the K296E rhodopsin mutant. (A) Confocal microscopy image of retinal cryosections from 2-week-old B6,  $Rho^{K296E/+}$  and  $Rho^{K296E}$  mice labeled with the anti-4D2 antibody (red). (B) Confocal microscopy image of retinal cryosections from 1-month-old  $Rho^{K296E/+}$  mice or 1-month- and 9-month-old  $Rho^{TgG90D}$  mice labeled with the anti-4D2 antibody or PROTEOSTAT (red). Nuclei are labeled with DAPI (blue). Confocal microscopy images of retinal cryosections were obtained at 40 $\times$  magnification. Rod outer segments (ROS), outer nuclear layer (ONL), inner nuclear layer (INL), and ganglion cell layer (GCL) are labeled. Scale bar, 50  $\mu$ m.

constitutively active rhodopsin mutants cause aggregation, and photoreceptor cell death caused by constitutively active rhodopsin mutants can have different molecular origins.

Higher magnification images were obtained of the outer nuclear layer to resolve the morphology of PROTEOSTAT labeling. PROTEOSTAT labeling surrounded photoreceptor cell nuclei (Figure 7A), which was the same labeling pattern displayed for misfolding mutants of rhodopsin that aggregate [7, 23]. PROTEOSTAT-positive nuclei were both relatively healthy with a single large central chromocenter and unhealthy with disrupted nuclei. Thus, the K296E rhodopsin mutant mislocalizes in photoreceptor cells and aggregates similarly to previously characterized misfolding mutants of rhodopsin. The appearance of PROTEOSTAT labeling surrounding photoreceptor cell nuclei can precede the deterioration of the nuclei.

### 3.5 | Relationship Between Aggregation and Photoreceptor Cell Death

To determine if the PROTEOSTAT-labeled aggregates contribute to photoreceptor cell death, the relationship between

aggregation, detected by PROTEOSTAT, and photoreceptor cell death, assessed by TUNEL, was determined. The level of TUNEL and PROTEOSTAT positive photoreceptor cell nuclei were quantified in the retina of mice at different ages. In  $Rho^{K296E/+}$  mice, the level of TUNEL and PROTEOSTAT positive photoreceptor cell nuclei appeared to be correlated, with the peak occurring at about 3 weeks of age (Figure 7B,C). In  $Rho^{K296E}$  mice, where photoreceptor cell loss is more severe, the level of TUNEL and PROTEOSTAT positive nuclei was higher than that observed in  $Rho^{K296E/+}$  mice. Thus, the level of photoreceptor cell death is related to the appearance of PROTEOSTAT-labeled photoreceptor cell nuclei. To determine further the relationship between photoreceptor cell death and aggregation, the level of colabeling of photoreceptor cell nuclei by TUNEL and PROTEOSTAT was determined (Figure 7D). At all ages of  $Rho^{K296E/+}$  mice tested, a majority of nuclei were co-labeled by TUNEL and PROTEOSTAT, whereas only a relatively few nuclei were labeled by TUNEL only (Figure 7E,F). Up to a quarter of nuclei were labeled only by PROTEOSTAT. Taken together, it appears that the appearance of aggregates surrounding photoreceptor cell nuclei can precede cell death and that these aggregates can contribute to the onset of cell death.

### 3.6 | In Vitro Characterization of Rhodopsin K296E Mutant Aggregates

To examine the propensity of K296E rhodopsin to aggregate and determine whether this is a species-specific property, a FRET-based method we developed to detect rhodopsin aggregates in HEK293 cells was used [17]. The K296E mutation was introduced on the murine, human, and bovine rhodopsin backgrounds. WT and mutant rhodopsins were tagged with either a yellow fluorescent protein (YFP) variant or mTurquoise2 (mTq2) [39, 40] and coexpressed in HEK293 cells. WT rhodopsin typically forms oligomers in photoreceptor cells [41]. The formation of oligomers and aggregates can be differentiated in our assay by the sensitivity of the FRET signal to the mild detergent *n*-dodecyl- $\beta$ -D-maltoside (DM), where DM-sensitive and DM-insensitive FRET derive from oligomers and aggregates, respectively. DM-sensitive and DM-insensitive FRET  $E_{max}$  was measured for WT and mutant rhodopsins (Figure 8A,B) from FRET curves generated by varying the ratios of YFP- and mTq2-tagged rhodopsins (Figure 8D). Only the specific FRET signal was considered since the physiological relevance of the FRET signal equal to or less than non-specific FRET is ambiguous [17].

For murine WT rhodopsin, only specific DM-sensitive FRET was detected, indicating that rhodopsin predominantly forms oligomers rather than aggregates in HEK293 cells (Figure 8C), as shown previously [7, 42]. For the K296E mutation on both murine and human rhodopsin backgrounds, only specific DM-insensitive FRET was detected, indicating that the mutants predominantly form aggregates in HEK293 cells. In contrast, the K296E mutation on a bovine rhodopsin background predominantly displayed specific DM-sensitive FRET with a small DM-insensitive FRET signal, indicating the mutant forms mostly oligomers and some aggregates. These in vitro studies demonstrate the propensity of the K296E mutation to promote rhodopsin aggregation is dependent on the species. Both murine and

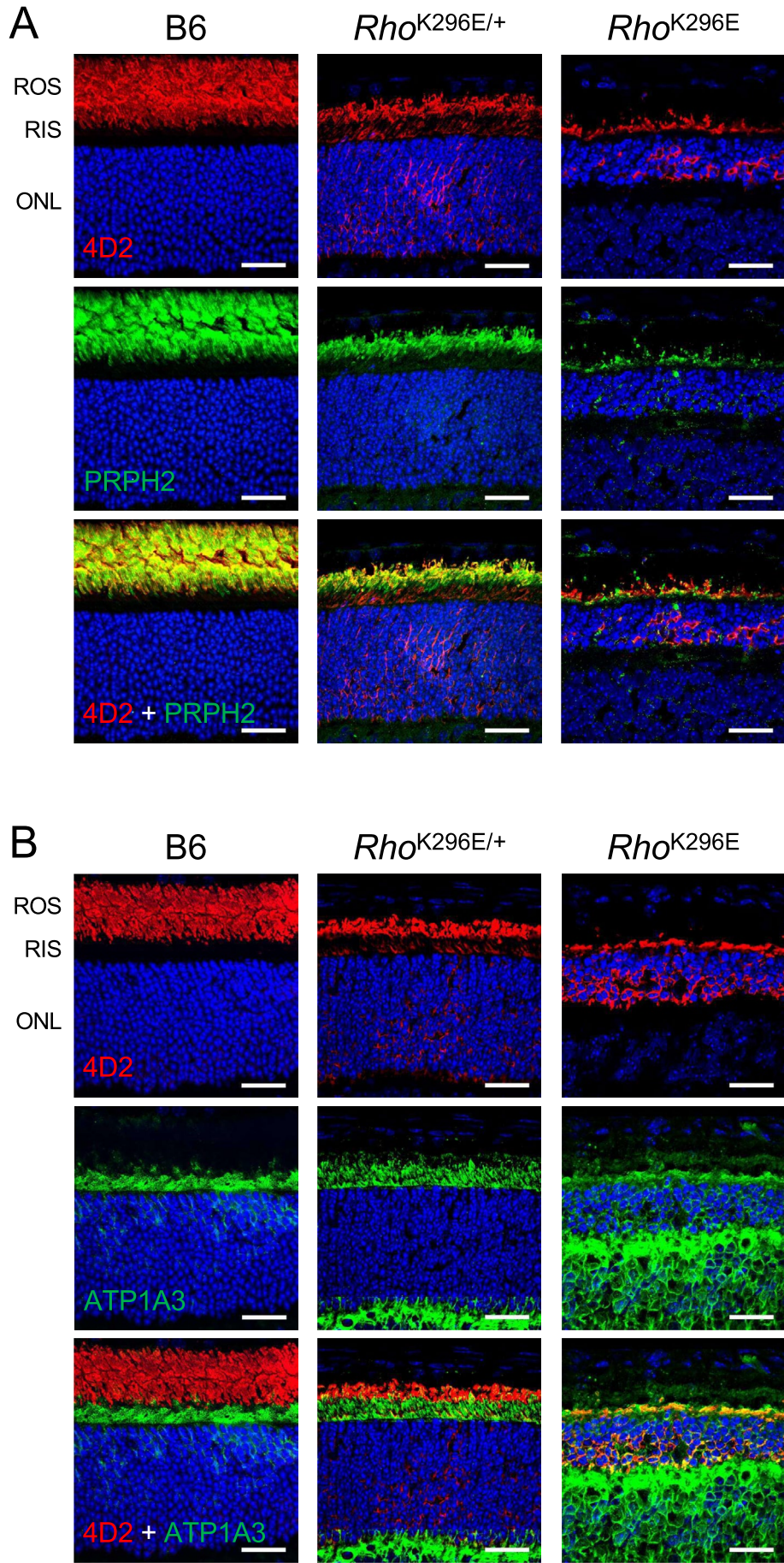


**FIGURE 6** | Legend on next page.

**FIGURE 6** | Localization of rhodopsin in rod outer and inner segments. Confocal microscopy image of retinal cryosections from 2-week-old B6, *Rho*<sup>K296E/+</sup> and *Rho*<sup>K296E</sup> mice either co-labeled with the anti-4D2 (red) and anti-PRPH2 (green) antibodies (A) or co-labeled with the anti-4D2 (red) and anti-ATP1A3 (green) antibodies (B). Nuclei are labeled with NucBlue (blue). Confocal microscopy images were obtained at 100× magnification and both separated and merged images are shown. Rod outer segments (ROS), rod inner segments (RIS), and outer nuclear layer (ONL) are labeled. Scale bar, 25 μm.

human K296E rhodopsin mutants are predicted to aggregate, which is consistent with studies in the K296E mutant rhodopsin knockin mice.

To determine whether the K296E mutant can physically interact with WT rhodopsin when coexpressed, as would occur in heterozygous *Rho*<sup>K296E/+</sup> mice, FRET curves were generated from cells coexpressing YFP-tagged K296E rhodopsin and mTq2-tagged WT rhodopsin on either murine or human backgrounds (Figure 8D). No specific DM-sensitive FRET and only a small specific DM-insensitive FRET signal were observed (Figure 8A,B), indicating the absence of physical interactions except for a minor fraction of the mutant that aggregates with WT rhodopsin. The aggregation represented by this small specific DM-insensitive FRET signal has previously been attributed to a minor population of misfolded WT rhodopsin that aggregates with the mutant *in vitro* that likely does not occur *in vivo* in photoreceptor cells [7, 42]. Thus, the K296E rhodopsin mutant is not predicted to interact with WT rhodopsin appreciably in photoreceptor cells of *Rho*<sup>K296E/+</sup> mice.

A K296M mutation, which also causes adRP and is predicted to promote constitutive activity in rhodopsin like the K296E mutation [43–45], was examined to determine whether this mutant aggregates like the K296E mutant. The K296M mutant on a human rhodopsin background predominantly displayed specific DM-insensitive FRET with a small DM-sensitive FRET signal (Figure 8A–C), indicating that this mutant forms mostly aggregates and some oligomers. Thus, the K296M mutation promotes the aggregation of rhodopsin like the K296E mutation; however, the aggregation is less severe, with a fraction of the mutant able to form oligomers.

## 4 | Discussion

Characterization of knockin mice expressing the K296E rhodopsin mutant has clarified two major questions about the K296E mutation. The first question is what is the molecular cause of photoreceptor cell death promoted by the mutation? The second question is why some constitutively active mutations cause RP whereas others cause CSNB? The predominant focus of the pathogenic mechanism of the K296E mutation has been on the effect or consequence of the constitutive activity of the receptor promoted by the mutation [12, 13]. We demonstrate here both *in vivo* and *in vitro* that the K296E rhodopsin mutant aggregates, and that aggregation can contribute to photoreceptor cell death.

Many early *in vitro* characterizations of the K296E mutation were conducted on a bovine rhodopsin background. The earliest study demonstrated that the mutant is constitutively active [11], which is a reason why this defect has been the primary focus when considering the pathogenic mechanism of the mutation. Later *in vitro* studies showed that while a large fraction

of the K296E rhodopsin mutant can fold properly, there were also indications that it may misfold and aggregate [16, 46]. We demonstrate here that the bovine rhodopsin background is a poor molecular model to examine the effect of mutation in rhodopsin to understand human disease. The K296E rhodopsin mutation promoted similar aggregation profiles on the murine and human rhodopsin backgrounds, where the mutants were predominantly aggregated (Figure 8C). The same mutation on the bovine rhodopsin background, however, resulted in a less severe aggregation profile where most of the mutant formed oligomers like it does in WT rhodopsin. We demonstrated previously that the aggregation profile of the P23H mutation on a bovine rhodopsin background is also less severe than on the human or murine rhodopsin backgrounds [7, 28]. While the molecular interactions stabilizing the structures of WT murine and bovine rhodopsin appear to be conserved [47], the impact of mutations differs on the two backgrounds. So far, it appears that *in vitro* properties of mutations in murine and human rhodopsin backgrounds are equivalent, thereby justifying the use of knockin mouse models to study rhodopsin-mediated adRP.

The K296E rhodopsin mutation shares some common properties as the P23H and G188R rhodopsin mutations, which are classified as mutations that cause receptor misfolding and aggregation and adRP [3, 7]. *Rho*<sup>K296E/+</sup> mice like *Rho*<sup>P23H/+</sup> and *Rho*<sup>G188R/+</sup> mice display progressive retinal degeneration where the inferior retina exhibits a more rapidly progressing degeneration compared to the superior retina and rod outer segments are shortened (Figures 4A,C and 6A). This differential severity in retinal degeneration in the inferior and superior regions of the retina is also observed in patients with adRP caused by misfolding rhodopsin mutations; however, the reason why this occurs is currently unresolved [48]. In knockin mice, all three mutants are shown to mislocalize in the photoreceptor cell and aggregate (Figure 5B) [7], as demonstrated by PROTEOSTAT labeling that surrounds the nuclei (e.g., Figure 7A). This labeling of photoreceptor cell nuclei has been demonstrated to derive from the aggregation of mutant rhodopsin [7]. In heterozygous mice, the K296E rhodopsin mutant is predicted not to appreciably interact with WT rhodopsin (Figure 8A,B), as was demonstrated previously for the P23H and G188R rhodopsin mutants [7]. Aggregation seems to be a major driver of photoreceptor cell death in mice expressing the K296E rhodopsin mutant since there were relatively few photoreceptor cells that were only TUNEL positive while most exhibited PROTEOSTAT labeling either alone or together with TUNEL labeling (Figure 7D–F). This pattern is also observed in *Rho*<sup>P23H/+</sup> and *Rho*<sup>G188R/+</sup> mice where aggregation is a major driver of photoreceptor cell death [23].

There are key differences exhibited by the K296E rhodopsin mutant that suggest aggregation may not be the sole contributor to photoreceptor cell loss. The level of both TUNEL and PROTEOSTAT positive cells is lower in mice expressing the K296E rhodopsin mutant compared to those expressing either

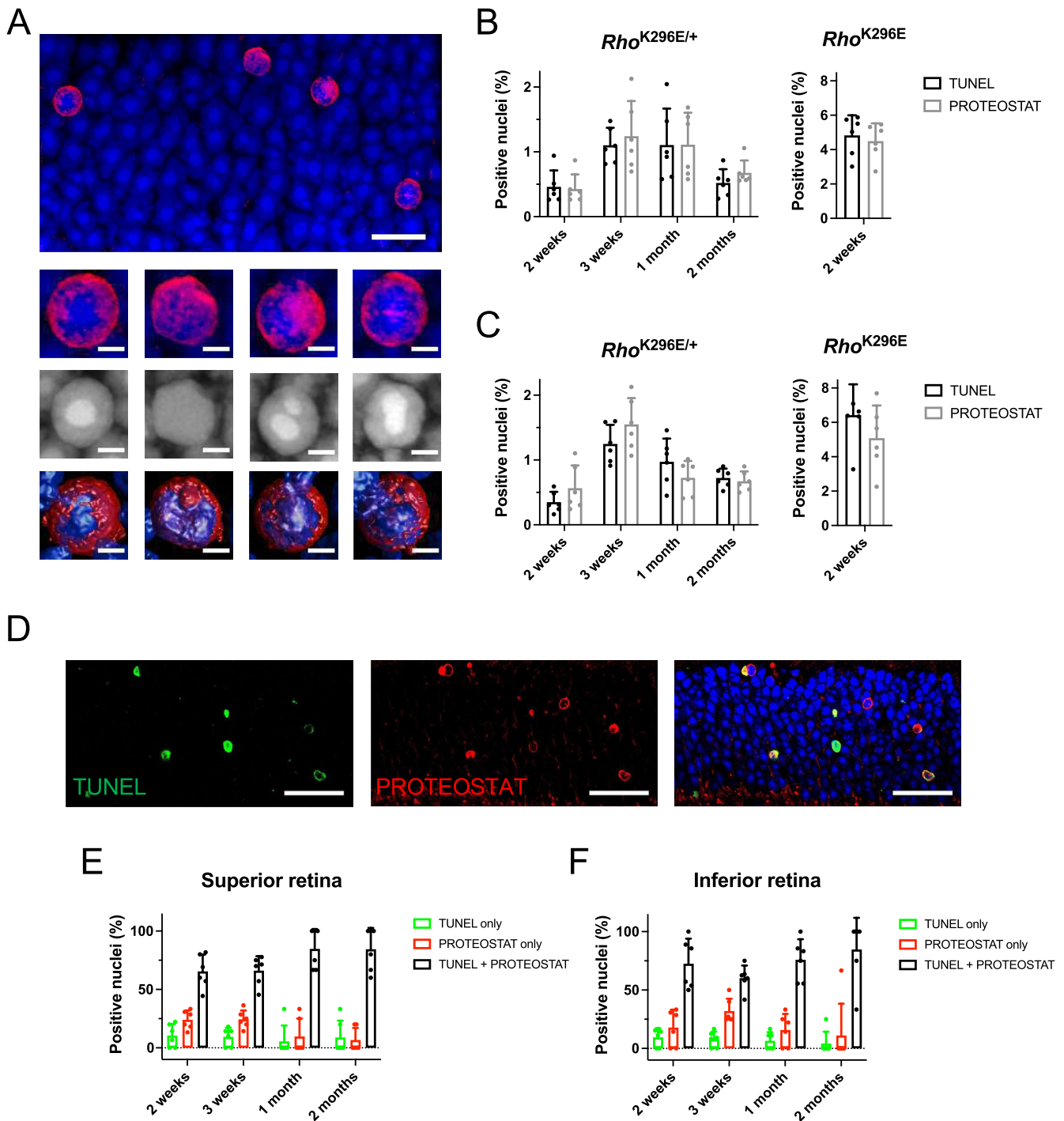


**FIGURE 7** | Relationship between PROTEOSTAT- and TUNEL-positive photoreceptor cells. (A) Maximum intensity projection image of retinal cryosection from 3-week-old *Rho*<sup>K296E/+</sup> mice labeled with PROTEOSTAT (red) and NucBlue (blue). Scale bar, 5  $\mu$ m. Maximum intensity projection image was generated using images obtained at 100 $\times$  magnification with 2.5 $\times$  digital zoom with deconvolution. Zoomed in images of PROTEOSTAT-positive nuclei are shown below along with a gray scale image of NucBlue staining only and a surface rendered image. Scale bar, 1  $\mu$ m. (B, C) The number of nuclei labeled by TUNEL (black) or PROTEOSTAT (gray) in the outer nuclear layer were quantified in the superior (B) and inferior (C) regions of the retina in *Rho*<sup>K296E/+</sup> and *Rho*<sup>K296E</sup> mice at the ages indicated. Individual data points are plotted along with the mean and standard deviation ( $n = 6$ ). (D) Confocal microscopy image of retinal cryosections from 3-week-old *Rho*<sup>K296E/+</sup> mice labeled with both PROTEOSTAT (red) and TUNEL (green). Nuclei are labeled with NucBlue (blue). Confocal microscopy images were obtained at 100 $\times$  magnification and both separated and merged images are shown. Scale bar, 25  $\mu$ m. (E, F) The number of photoreceptor cell nuclei labeled by TUNEL (green) or PROTEOSTAT (red) alone or co-labeled with TUNEL and PROTEOSTAT (black) were quantified from confocal microscopy images of retinal cryosections taken from *Rho*<sup>K296E/+</sup> mice (e.g., Figure 7D) at the ages indicated. Individual data points are plotted along with the mean and standard deviation ( $n = 6$ ).

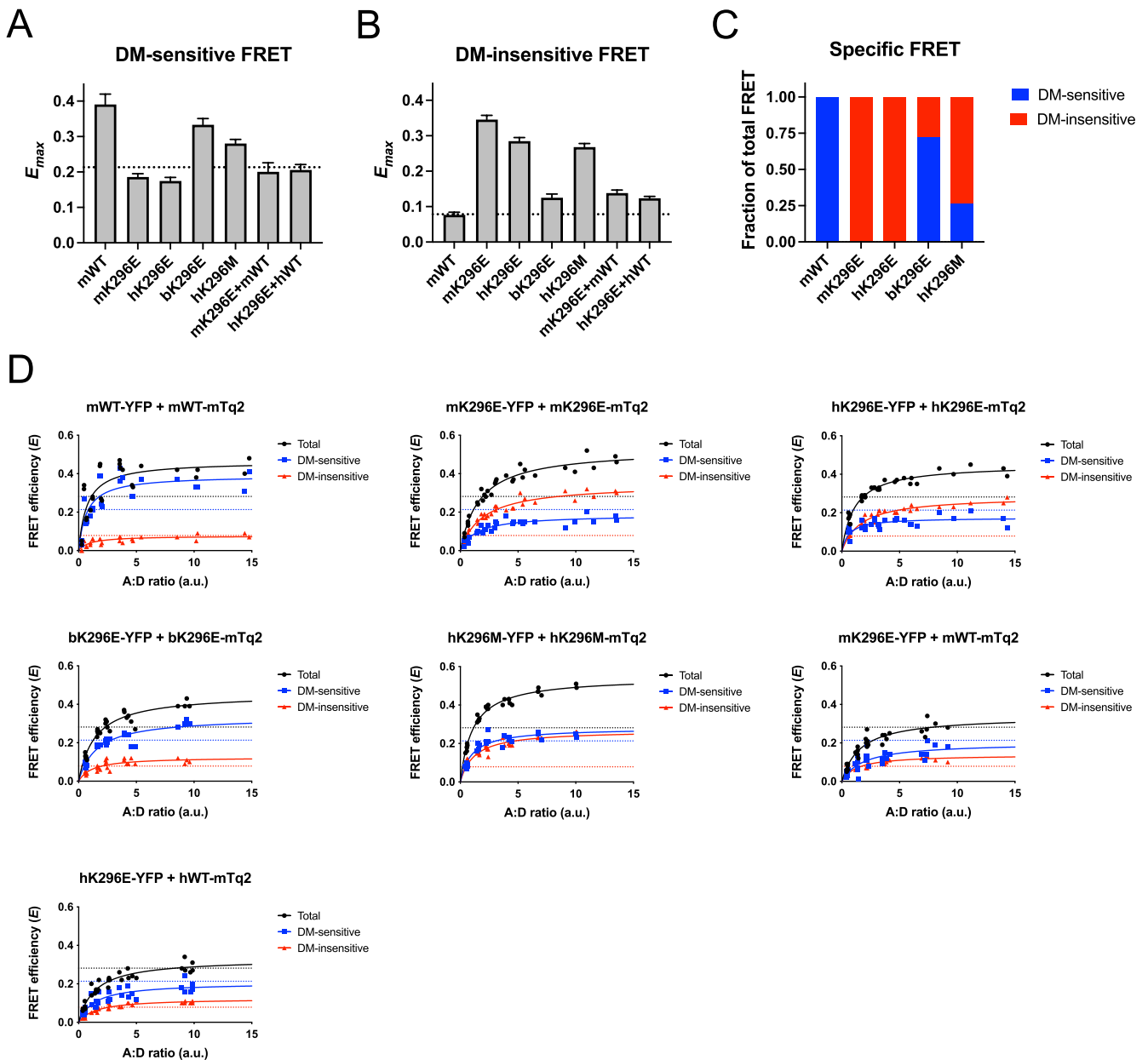


**FIGURE 8** | Aggregation properties of the K296E and K296M rhodopsin mutants. (A, B) FRET was conducted on HEK293 cells expressing YFP- and mTq2-tagged WT murine rhodopsin, murine (mK296E), human (hK296E), or bovine (bK296E) rhodopsin with the K296E mutation, or human rhodopsin with the K296M mutation (hK296M). FRET was also conducted on HEK293 cells coexpressing YFP-tagged K296E rhodopsin and mTq2-tagged WT rhodopsin on murine (mK296E + mWT) or human (hK296E + hWT) backgrounds. Fitted values of the maximal FRET efficiency ( $E_{max}$ ) and the standard errors from the fits are shown for DM-sensitive (A) and DM-insensitive (B) components of generated FRET curves (D). The non-specific  $E_{max}$ , defined previously from FRET curves generated from HEK293 cells coexpressing YFP-tagged WT rhodopsin and mTq2-tagged m2 muscarinic receptor [27], is indicated by the dotted lines. All fitted parameters are reported in Table S6. (C) The fraction of the total FRET derived from DM-sensitive (blue) and DM-insensitive (red) FRET is shown for each of the rhodopsins examined. Only the specific FRET signal was considered. (D) FRET curves were generated from cells expressing the indicated YFP-tagged and mTq2-tagged murine WT (mWT), murine K296E (mK296E), human K296E (hK296E), bovine K296E (bK296E), human K296M (hK296M), or human WT (hWT) rhodopsins. Total (black), DM-sensitive (blue), and DM-insensitive (red) FRET curves are shown. Each curve contains data from 6 separate experiments, which were combined and simultaneously fit with a rectangular hyperbolic function. Fitted lines are shown and values obtained from fits are reported in (A, B) and Table S6. The non-specific  $E_{max}$  is indicated by the dashed lines.

the P23H or G188R rhodopsin mutants [7]. Despite the lower levels of TUNEL and PROTEOSTAT positive cells, the rate of photoreceptor cell loss in  $Rho^{K296E/+}$  mice is similar to that in  $Rho^{G188R/+}$  mice and faster than that in the  $Rho^{P23H/+}$  mice (Figure S3). The severity of photoreceptor cell loss in  $Rho^{K296E/+}$

mice is also reflected in the ERG response, where the functional deficit in  $Rho^{K296E/+}$  mice is similar to that in  $Rho^{G188R/+}$  mice but greater than that in the  $Rho^{P23H/+}$  mice (Figure 4D–F) [7]. A variety of cell death mechanisms have been proposed for rhodopsin-mediated photoreceptor cell death [49]. TUNEL

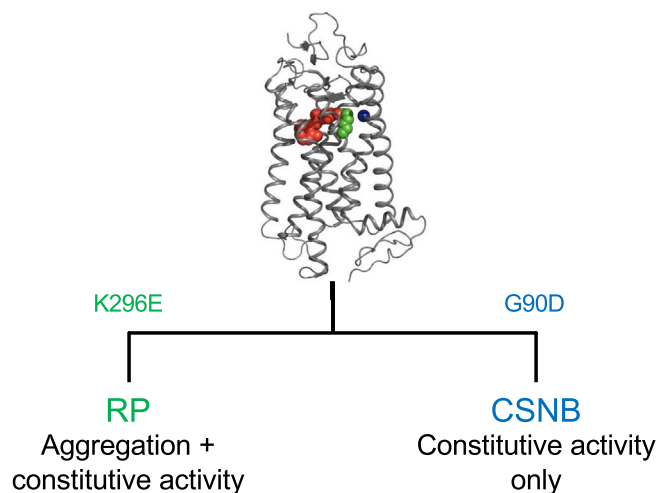


**FIGURE 9** | Differentiation between constitutively active mutants causing RP and CSNB. Studies here suggest that constitutively active mutants that cause the more severe phenotypes in RP may aggregate (e.g., K296E) whereas constitutively active mutants causing the less severe phenotypes in CSNB do not (e.g., G90D). The crystal structure of rhodopsin (PDB ID: 1U19) is shown highlighting G90 (blue), K296 (green), and 11-*cis* retinal (red) as spheres.

staining is indicative of apoptosis, but other cell death mechanisms may also be detected by TUNEL albeit with variable efficiency [50]. Since TUNEL positive cells are lower in *Rho*<sup>K296E/+</sup> mice but the rate of photoreceptor cell loss is similar or greater than that in *Rho*<sup>P23H/+</sup> and *Rho*<sup>G188R/+</sup> mice, this discrepancy may point to an additional cell death mechanism to the one promoted by rhodopsin aggregation with different kinetics or TUNEL staining efficiency.

The additional cell death mechanism may be a byproduct of the originally attributed constitutive activity promoted by the K296E rhodopsin mutation, which results in stable interactions of the mutant with arrestin [12, 13]. Previous studies suggest that the constitutively active mutant folds properly but is retained in the rod inner segment and outer nuclear layer because it forms a stable complex with arrestin [12]. Observations in *Rho*<sup>K296E</sup> mice are consistent with this view. In *Rho*<sup>K296E</sup> mice, the mutant is mislocalized in the rod inner segment and outer nuclear layer and is largely unable to promote the formation of the rod outer segment (Figure 6). Some of the mutant appears to fold properly since western blots of retinal extracts from *Rho*<sup>K296E</sup> mice display a band corresponding to the monomeric receptor species (Figure 3E), which would not be present if the mutant were fully aggregated, as shown previously for the G188R and P23H rhodopsin mutants, which migrate as dimeric or larger species in western blots [7, 42]. Thus, there appears to be a population of the K296E rhodopsin mutant that is properly folded and likely constitutively active.

Studies here also provide an explanation of why different constitutively active mutants are classified as a cause of different diseases. One class of constitutively active mutations (G90V, S186W, D190N, K296E, K296M) is classified as a cause of RP, which causes a more severe retinal degeneration phenotype, whereas another class of constitutively active mutations (G90D, T94I, A292E, A295V) is classified as a cause of CSNB,

which causes a milder phenotype of night blindness originally thought to be without retinal degeneration [8]. It was shown later on that the G90D rhodopsin mutation can cause mild retinal degeneration in both mice and patients [20, 38]. Nonetheless, we demonstrate here that the G90D rhodopsin mutant causes retinal degeneration in an aggregation independent manner (Figure 5B). Thus, the distinction between constitutively active mutants classified as a cause of RP versus those that cause CSNB may be the ability of the mutants to form aggregates for the former but not the latter (Figure 9). In support of this hypothesis, we also demonstrated that the constitutively active K296M rhodopsin mutant aggregates *in vitro* (Figure 8A–C) and the constitutively active D190N rhodopsin mutant has previously been shown to form aggregates detectable by PROTEOSTAT *in vivo* [51].

The severity of the retinal degeneration phenotype appears to be related to the expression level of the K296E rhodopsin mutant. The thymine to guanine nucleotide mutation in the NRE *cis*-regulatory element of the rhodopsin promoter, which is present in line K29-1 (Figure 1B,C), has been studied previously in an *in vivo* reporter-based assay and is predicted to decrease the expression of rhodopsin [52]. While the expression of the K296E rhodopsin mutant does appear to be affected by the mutation in the promoter region, the magnitude of the effect is unclear. In homozygous mice of line K29-1, expression of the mutant is affected (Figure 3F), although effects at the level of transcription are obscured because of retinal degeneration in the other lines. In heterozygous mice of line K29-1, no difference is observed in the expression of rhodopsin at both transcript and protein levels (Figure 3A,C), which may indicate the presence of compensatory mechanisms and a more modest change in the expression of rhodopsin due to the mutation in the promoter region. Regardless of the magnitude of the effect of the mutation in the promoter region on the expression of the K296E rhodopsin mutant, much of the mutant appears to be degraded as it is in knockin mice expressing the P23H and G188R rhodopsin mutants [7].

In summary, we demonstrate here that the constitutively active K296E rhodopsin mutation causes aggregation of the receptor, which appears to contribute to photoreceptor cell death. Over half of rhodopsin mutations causing adRP have already been shown to cause receptor misfolding and aggregation, and it now appears there are even more since mutations classified in other categories may also cause misfolding and aggregation. We demonstrate that reducing the expression of the mutant can improve the retinal degeneration phenotype, which indicates that therapeutic strategies targeting the expression of the mutant may be beneficial. Lastly, studies here indicate that the differentiation of constitutively active rhodopsin mutants as a cause of RP or CSNB may be based on whether the mutation can also promote receptor aggregation (Figure 9).

#### Author Contributions

S.V. and V.P. conducted experiments and edited the manuscript. S.V., V.P., and P.S.-H.P. designed experiments and analyzed data. P.S.-H.P. wrote the manuscript.

## Acknowledgments

We thank John Denker for generating DNA constructs, genotyping mice, sequencing DNA, testing sgRNA for cutting efficiency, and validating knockin mice, Heather Butler for breeding and maintaining mouse colonies, Dawn Smith for culturing HEK293 cells and generating cryosections, Catherine Doller for generating cryosections, and Maryanne Pendergast for help with microscopy and processing of images. We thank the Case Transgenic and Targeting Facility and the Genomics Core at Case Western Reserve University School of Medicine (Cleveland, OH) for generating and identifying K296E rhodopsin knockin mice. This work was funded by grants from the National Institutes of Health (R01EY021731, P30EY011373, and UL1RR024989).

## Conflicts of Interest

The authors declare no conflicts of interest.

## Data Availability Statement

All data supporting the findings of this study are available within the paper and in [Supporting Information](#) files. Raw data are available from the corresponding author upon reasonable request.

## References

1. D. Meng, S. D. Ragi, and S. H. Tsang, "Therapy in Rhodopsin-Mediated Autosomal Dominant Retinitis Pigmentosa," *Molecular Therapy* 28 (2020): 2139–2149.
2. D. T. Hartong, E. L. Berson, and T. P. Dryja, "Retinitis Pigmentosa," *Lancet* 368 (2006): 1795–1809.
3. D. Athanasiou, M. Aguila, J. Bellingham, et al., "The Molecular and Cellular Basis of Rhodopsin Retinitis Pigmentosa Reveals Potential Strategies for Therapy," *Progress in Retinal and Eye Research* 62 (2018): 1–23.
4. M. P. Krebs, D. C. Holden, P. Joshi, C. L. Clark, 3rd, A. H. Lee, and S. Kaushal, "Molecular Mechanisms of Rhodopsin Retinitis Pigmentosa and the Efficacy of Pharmacological Rescue," *Journal of Molecular Biology* 395 (2010): 1063–1078.
5. A. Gal, E. Apfelstedt-Sylla, A. R. Janecke, and E. Zrenner, "Rhodopsin Mutations in Inherited Retinal Dystrophies and Dysfunctions," *Progress in Retinal and Eye Research* 16 (1997): 51–79.
6. T. P. Dryja, T. L. McGee, E. Reichel, et al., "A Point Mutation of the Rhodopsin Gene in One Form of Retinitis Pigmentosa," *Nature* 343 (1990): 364–366.
7. S. Vasudevan, S. Senapati, M. Pendergast, and P. S. Park, "Aggregation of Rhodopsin Mutants in Mouse Models of Autosomal Dominant Retinitis Pigmentosa," *Nature Communications* 15 (2024): 1451.
8. P. S. Park, "Constitutively Active Rhodopsin and Retinal Disease," *Advances in Pharmacology* 70 (2014): 1–36.
9. T. J. Keen, C. F. Inglehearn, D. H. Lester, et al., "Autosomal Dominant Retinitis Pigmentosa: Four New Mutations in Rhodopsin, One of Them in the Retinal Attachment Site," *Genomics* 11 (1991): 199–205.
10. S. L. Owens, F. W. Fitzke, C. F. Inglehearn, et al., "Ocular Manifestations in Autosomal Dominant Retinitis Pigmentosa With a Lys-296-Glu Rhodopsin Mutation at the Retinal Binding Site," *British Journal of Ophthalmology* 78 (1994): 353–358.
11. P. R. Robinson, G. B. Cohen, E. A. Zhukovsky, and D. D. Oprian, "Constitutively Active Mutants of Rhodopsin," *Neuron* 9 (1992): 719–725.
12. J. Chen, G. Shi, F. A. Concepcion, G. Xie, D. Oprian, and J. Chen, "Stable Rhodopsin/Arrestin Complex Leads to Retinal Degeneration in a Transgenic Mouse Model of Autosomal Dominant Retinitis Pigmentosa," *Journal of Neuroscience* 26 (2006): 11929–11937.
13. T. Li, W. K. Franson, J. W. Gordon, E. L. Berson, and T. P. Dryja, "Constitutive Activation of Phototransduction by K296E Opsin Is Not a Cause of Photoreceptor Degeneration," *Proceedings of the National Academy of Sciences of the United States of America* 92 (1995): 3551–3555.
14. E. Brill, K. M. Malanson, R. A. Radu, et al., "A Novel Form of Transducin-Dependent Retinal Degeneration: Accelerated Retinal Degeneration in the Absence of Rod Transducin," *Investigative Ophthalmology & Visual Science* 48 (2007): 5445–5453.
15. W. C. Chiang, N. Hiramoto, C. Messah, H. Kroeger, and J. H. Lin, "Selective Activation of ATF6 and PERK Endoplasmic Reticulum Stress Signaling Pathways Prevent Mutant Rhodopsin Accumulation," *Investigative Ophthalmology & Visual Science* 53 (2012): 7159–7166.
16. R. S. Saliba, P. M. Munro, P. J. Luthert, and M. E. Cheetham, "The Cellular Fate of Mutant Rhodopsin: Quality Control, Degradation and Aggresome Formation," *Journal of Cell Science* 115 (2002): 2907–2918.
17. M. Gragg and P. S. Park, "Detection of Misfolded Rhodopsin Aggregates in Cells by Forster Resonance Energy Transfer," *Methods in Cell Biology* 149 (2019): 87–105.
18. P. A. Sieving, M. L. Fowler, R. A. Bush, et al., "Constitutive 'Light' Adaptation in Rods From G90D Rhodopsin: A Mechanism for Human Congenital Nightblindness Without Rod Cell Loss," *Journal of Neuroscience* 21 (2001): 5449–5460.
19. S. Senapati, M. Gragg, I. S. Samuels, V. M. Parmar, A. Maeda, and P. S. Park, "Effect of Dietary Docosahexaenoic Acid on Rhodopsin Content and Packing in Photoreceptor Cell Membranes," *Biochimica et Biophysica Acta* 1860 (2018): 1403–1413.
20. A. T. Colozo, S. Vasudevan, and P. S. Park, "Retinal Degeneration in Mice Expressing the Constitutively Active G90D Rhodopsin Mutant," *Human Molecular Genetics* 29 (2020): 881–891.
21. R. S. Molday and D. MacKenzie, "Monoclonal Antibodies to Rhodopsin: Characterization, Cross-Reactivity, and Application as Structural Probes," *Biochemistry* 22 (1983): 653–660.
22. S. Vasudevan, I. S. Samuels, and P. S. Park, "Gpr75 Knockout Mice Display Age-Dependent Cone Photoreceptor Cell Loss," *Journal of Neurochemistry* 167 (2023): 538–555.
23. S. Vasudevan and P. S. Park, "A Y178C Rhodopsin Mutation Causes Aggregation and Comparatively Severe Retinal Degeneration," *Cell Death Discovery* 11 (2025): 32.
24. C. A. Schneider, W. S. Rasband, and K. W. Eliceiri, "NIH Image to ImageJ: 25 Years of Image Analysis," *Nature Methods* 9 (2012): 671–675.
25. J. Schindelin, I. Arganda-Carreras, E. Frise, et al., "Fiji: An Open-Source Platform for Biological-Image Analysis," *Nature Methods* 9 (2012): 676–682.
26. L. M. Miller, M. Gragg, T. G. Kim, and P. S. Park, "Misfolded Opsin Mutants Display Elevated Beta-Sheet Structure," *FEBS Letters* 589 (2015): 3119–3125.
27. M. Gragg and P. S. Park, "Misfolded Rhodopsin Mutants Display Variable Aggregation Properties," *Biochimica et Biophysica Acta* 1864 (2018): 2938–2948.
28. S. Vasudevan and P. S. Park, "Differential Aggregation Properties of Mutant Human and Bovine Rhodopsin," *Biochemistry* 60 (2021): 6–18.
29. S. Sakami, T. Maeda, G. Bereta, et al., "Probing Mechanisms of Photoreceptor Degeneration in a New Mouse Model of the Common Form of Autosomal Dominant Retinitis Pigmentosa due to P23H Opsin Mutations," *Journal of Biological Chemistry* 286 (2011): 10551–10567.
30. M. E. Breton, A. W. Schueller, T. D. Lamb, and E. N. Pugh, Jr., "Analysis of ERG a-Wave Amplification and Kinetics in Terms of the G-Protein Cascade of Phototransduction," *Investigative Ophthalmology & Visual Science* 35 (1994): 295–309.

31. D. C. Hood and D. G. Birch, "The A-Wave of the Human Electroretinogram and Rod Receptor Function," *Investigative Ophthalmology & Visual Science* 31 (1990): 2070–2081.
32. A. E. Weymouth and A. J. Vingrys, "Rodent Electroretinography: Methods for Extraction and Interpretation of Rod and Cone Responses," *Progress in Retinal and Eye Research* 27 (2008): 1–44.
33. D. Hicks and R. S. Molday, "Differential Immunogold-Dextran Labeling of Bovine and Frog Rod and Cone Cells Using Monoclonal Antibodies Against Bovine Rhodopsin," *Experimental Eye Research* 42 (1986): 55–71.
34. L. L. Molday, C. L. Cheng, and R. S. Molday, "Cell-Specific Markers for the Identification of Retinal Cells and Subcellular Organelles by Immunofluorescence Microscopy," *Methods in Molecular Biology* 1834 (2019): 293–310.
35. D. Shen, J. Coleman, E. Chan, et al., "Novel Cell- and Tissue-Based Assays for Detecting Misfolded and Aggregated Protein Accumulation Within Aggresomes and Inclusion Bodies," *Cell Biochemistry and Biophysics* 60 (2011): 173–185.
36. P. A. Sieving, J. E. Richards, F. Naarendorp, E. L. Bingham, K. Scott, and M. Alpern, "Dark-Light: Model for Nightblindness From the Human Rhodopsin Gly-90->Asp Mutation," *Proceedings of the National Academy of Sciences of the United States of America* 92 (1995): 880–884.
37. V. R. Rao, G. B. Cohen, and D. D. Oprian, "Rhodopsin Mutation G90D and a Molecular Mechanism for Congenital Night Blindness," *Nature* 367 (1994): 639–642.
38. N. Kobal, T. Krasovec, M. Sustar, et al., "Stationary and Progressive Phenotypes Caused by the p.G90D Mutation in Rhodopsin Gene," *International Journal of Molecular Sciences* 22 (2021): 2133.
39. G. J. Kremers, J. Goedhart, E. B. van Munster, and T. W. Gadella, Jr., "Cyan and Yellow Super Fluorescent Proteins With Improved Brightness, Protein Folding, and FRET Forster Radius," *Biochemistry* 45 (2006): 6570–6580.
40. J. Goedhart, D. von Stetten, M. Noirclerc-Savoie, et al., "Structure-Guided Evolution of Cyan Fluorescent Proteins Towards a Quantum Yield of 93%," *Nature Communications* 3 (2012): 751.
41. P. S. Park, "Supramolecular Organization of Rhodopsin in Rod Photoreceptor Cell Membranes," *Pflügers Archiv / European Journal of Physiology* 473 (2021): 1361–1376.
42. M. Gragg, T. G. Kim, S. Howell, and P. S. Park, "Wild-Type Opsin Does Not Aggregate With a Misfolded Opsin Mutant," *Biochimica et Biophysica Acta* 1858 (2016): 1850–1859.
43. J. M. Sullivan, K. M. Scott, H. F. Falls, J. E. Richards, and P. A. Sieving, "A Novel Rhodopsin Mutation at the Retinal Binding Site (Lys-296-Met) in ADRP," *Investigative Ophthalmology & Visual Science* 34 (1993): 1149.
44. T. Yang, B. B. Snider, and D. D. Oprian, "Synthesis and Characterization of a Novel Retinylamine Analog Inhibitor of Constitutively Active Rhodopsin Mutants Found in Patients With Autosomal Dominant Retinitis Pigmentosa," *Proceedings of the National Academy of Sciences of the United States of America* 94 (1997): 13559–13564.
45. J. Rim and D. D. Oprian, "Constitutive Activation of Opsin: Interaction of Mutants With Rhodopsin Kinase and Arrestin," *Biochemistry* 34 (1995): 11938–11945.
46. S. Kaushal and H. G. Khorana, "Structure and Function in Rhodopsin. 7. Point Mutations Associated With Autosomal Dominant Retinitis Pigmentosa," *Biochemistry* 33 (1994): 6121–6128.
47. S. Kawamura, A. T. Colozo, D. J. Muller, and P. S. Park, "Conservation of Molecular Interactions Stabilizing Bovine and Mouse Rhodopsin," *Biochemistry* 49 (2010): 10412–10420.
48. S. G. Jacobson, D. B. McGuigan, 3rd, A. Sumaroka, et al., "Complexity of the Class B Phenotype in Autosomal Dominant Retinitis Pigmentosa due to Rhodopsin Mutations," *Investigative Ophthalmology & Visual Science* 57 (2016): 4847–4858.
49. M. Azam and B. Jastrzebska, "Mechanisms of Rhodopsin-Related Inherited Retinal Degeneration and Pharmacological Treatment Strategies," *Cells* 14 (2025): 49.
50. S. Kari, K. Subramanian, I. A. Altomonte, A. Murugesan, O. Yli-Harja, and M. Kandhavelu, "Programmed Cell Death Detection Methods: A Systematic Review and a Categorical Comparison," *Apoptosis* 27 (2022): 482–508.
51. D. Silverman, Z. Chai, W. W. S. Yue, et al., "Dark Noise and Retinal Degeneration From D190N-Rhodopsin," *Proceedings of the National Academy of Sciences of the United States of America* 117 (2020): 23033–23043.
52. J. C. Kwasnieski, I. Mogno, C. A. Myers, J. C. Corbo, and B. A. Cohen, "Complex Effects of Nucleotide Variants in a Mammalian Cis-Regulatory Element," *Proceedings of the National Academy of Sciences of the United States of America* 109 (2012): 19498–19503.

### Supporting Information

Additional supporting information can be found online in the Supporting Information section.